JOURNAL OF GEOPHYSICAL RESEARCH, VOL. 99, NO. C4, PAGES 7945–7950, APRIL 15, 1994

Remote sensing of ocean waves: The Surface Wave Process Program experiment

R. M. Goldstein and F. Li
Jet Propulsion Laboratory, California Institute of Technology, Pasadena

J. Smith, R. Pinkel, and T. P. Barnett
Scripps Institution of Oceanography, La Jolla, California

Abstract. An airborne synthetic aperture radar (SAR) has been used as an interferometer to obtain direct, calibrated measurements of the ocean wind wave directional spectrum. Flights over the same area from three different directions produced reasonably consistent results. The SAR-derived wave data agree well with simultaneous observations by a conventional wave measuring system and with a novel in situ acoustic Doppler system.

1. Introduction

Measuring the directional properties of wind-generated waves in the open ocean from a surface platform is a difficult task under good weather conditions, and even more difficult in stormy conditions. Not surprisingly, several techniques for remotely sensing wave properties have been developed [*Jackson*, 1981; *Walsh et al.*, 1985], one of the most interesting of which is the synthetic aperture radar.

We have found that by using dual antennas to receive a standard SAR signal, we can measure wave heights without knowing the relationship between radar brightness and wave height [*Alpers et al.*, 1981; *Hasselmann et al.*, 1985; *Raney*, 1981]. The phase difference between the images from each antenna forms an interferogram that is directly proportional to the line-of-sight component of the velocity field at the ocean's surface. This information can be converted to calibrated directional wave estimates, as we shall show.

The following sections of this paper describe first the principals of radar interferometry and of the in situ acoustic Doppler system, and second the experimental setup and results from both remote wave-measuring systems are presented.

2. Remote Sensing Methods

2.1. Interferometry

Currents associated with larger gravity waves, internal waves, and other oceanic phenomena are visible to conventional and interferometric microwave radar only in their ability to modulate the surface Bragg waves, which are the principal scatterers seen by the radar [*Stewart*, 1985]. Thus the synthetic aperture radar (SAR) image intensity is not easily related to ocean wave height.

Interferometry is an extension of synthetic aperture radar which enables measurement of the line-of-sight velocity of each resolution element in the scene. The central idea is to use two receiving antennas, spaced collinearly along an aircraft (or satellite) flight path, each connected to separate receivers and yielding separate radar images. The phase difference between corresponding pixels in the two images is then a direct measure of the distance which the resolution element moved in the time between observations.

The interferometric technique measures the algebraic sum of small displacements (with respect to time) of the Bragg waves, such as the phase velocity of the Bragg waves themselves, the orbital velocity associated with the swell upon which they ride, and any underlying current that may be present. In our earlier work, we effectively removed the ocean wave information by averaging over large areas equivalent to many ocean wave lengths, which left only the ocean current information [*Goldstein et al.*, 1989].

In this study the orbital motion components due to the wind waves are separated from the Bragg phase velocity and the ocean currents (and saved) on the basis of their spatial frequencies. The Bragg and the ocean current velocities are usually steady over large areas of the scene, whereas the swell is composed of the higher spatial frequencies that are of interest in the ocean wave spectra. We note that the Bragg waves are not imaged directly as waves; rather, they provide the field of scatterers for the radar return. Because the interferometer measures directly the line-of-sight velocity, independent of such variables as radar power, antenna gain, surface reflectance, etc., it enables the determination of the actual height of the ocean waves via linear wave theory.

2.2. Acoustic Doppler Measurement Technique

Currents can also be measured just below the ocean surface using sound [*Emmanuel and Mandics*, 1973; *Pinkel and Speiss*, 1976]. The essence of the technique is to transmit acoustic pulses of known frequency and to measure the Doppler shift of sound backscattered from particles in the water. For pulses of finite duration, the distance from which the sound is returning at each instant is proportional to the time since the transmission. Thus the radial component of the water velocity is estimated as a function of radial distance from the device.

For sound returning from near the surface and with winds over about 3 m s^{-1}, the dominant scatterers are bubbles injected by breaking waves. The intensity of the backscatter from bubbles can vary by a factor of 1000, but the bubbles

Paper number 93JC03332.
0148-0227/94/93JC-03332$05.00

are strongly surface trapped both inside and outside the denser bubble clouds. The profile is thought to be roughly exponential, with a depth scale of the order of 1 to 1.5 m [*Thorpe*, 1986; *Crawford and Farmer*, 1987]. This "bubble layer" is continuous in winds over 3 or 4 m s^{-1}. This depth profile, combined with the acoustic beam pattern, determines the vertical weighting of the sonar measurements.

The sonar used for the present comparison was designed and operated specifically to monitor surface velocities in order to track both surface wave directional spectra and lower-frequency motions [*Smith*, 1989, 1992]. The system uses beam patterns which are narrow azimuthally but broad in the vertical direction (about 2/3° × 22° beam widths). Thus the Doppler shift of the returning sound indicates the velocity of fluid averaged over a volume determined by the range gating, the distance interval set by the length of the transmitted pulse, and the depth of the bubble layer. For the present system, these come to about 3 m in range by 2/3° in azimuth (3 m wide at 250 m range) by 2 or 3 m in depth. The resulting measurements are "semi-Lagrangian," following fluid parcels in the vertical but not in the horizontal directions. This beam geometry also minimizes sensitivity to pitch and roll of the platform.

Velocity estimates were formed by the standard complex autocovariance technique [*Miller and Rochwarger*, 1972], as modified for incoherent, repeat sequence coded sonars [*Pinkel and Smith*, 1992]. The sonars transmitted a 4-bit repeat sequence code every 3/4 s, with a center frequency of 195 kHz. Usable returns were obtained from as far as 400 m away. Covariance estimates were averaged in range for 4 ms (3 m), yielding an estimated rms error of about 10 cm s^{-1} in each range bin per transmission (ping). The total system consisted of 4 beams aimed at 45° increments.

3. Experimental Setup

The capabilities of an airborne, interferometric radar to measure accurately the ocean wave spectra were tested during the Surface Wave Process Program (SWAPP) [e.g., *Weller et al.*, 1991]. The experiment site was located 500 km off the central California coast, near 35°N, 127°W. Much of the experiment centered around the research floating instrument platform (FLIP) which provided estimates of the wave field with a conventional wave staff and the acoustic Doppler system [*Pinkel*, 1981; *Smith*, 1989, 1992]. Test flights were performed over FLIP at three different aircraft headings: 112°, 202°, and 247°. These headings are separated by 90° and 45° so that waves that are traveling, say, in the along-track direction in one pass would be traveling in the across-track direction in another pass. Thus we have tested the sensitivity of the measurements to the ocean wave direction. FLIP instruments obtained wave field measurements nearly continuously over the 22 days on location, including the times of the aircraft overflights.

The radar used in this study was installed on a NASA DC-8 aircraft operated by the Ames Research Center and stationed at Moffett Field, California. The essential characteristics of the radar are included in Table 1. Additional detail can be found in the work by *Goldstein and Zebker* [1987].

Table 1. Observations and Radar Parameters

	Ground Track, deg			
	202	247	112	FLIP
Wave Period, s	13.1	13.5	14.6	13
Wavelength, m	268	285	332	266
Wave direction, deg	107	116	95	110*
Wave height, m (RMS)	0.17	0.18	0.26	0.21

FLIP, floating instrument platform; wavelength, 24 cm; aircraft altitude, 8158 m; aircraft velocity, 217 m s^{-1}; antenna spacing, 19.3 m; along-track pixel spacing, 12.1 m; across-track pixel spacing, 8.2 m; image size, 12.4 × 7.5 km; range to image center, 12804 m; effective resolution, 24 m.

*Directional data from the Doppler sonar; wave period, wavelength, and height from the wave staff.

4. Radar Results

Plate 1 is a typical interferogram of the SWAPP scene. It was obtained by processing the received signals from each antenna into complex images. The phase difference between the two images formed the interferogram.

The phases differences are portrayed in the form of color. Light blue is used to show zero line-of-sight velocity. The color shades to green and yellow for motion away from the aircraft, and violet to magenta represents motion toward the aircraft. As noted earlier, only the line-of-sight component of the velocity is observed. The phase excursions of Plate 1 never exceed $\pm\pi$, so that the phase unwrapping problem does not occur in these data. The "brightness" of this image corresponds to the received power but with much reduced contrast, so that the elements of the SWAPP fleet can be seen (the four bright spots in the lower left of the image).

The presence of the gentle swell conditions that prevailed during this overflight is clearly seen in the interferogram. This is quantified by the two-dimensional spectrum of the phase (only) of the interferogram and is presented in Plate 2. It is composed of the (spatial) average of magnitude squares of 16 contiguous subspectra. Each subspectrum is the discrete Fourier transform of an area of dimension 128 × 128 pixels (about 1000 m × 1500 m). The two bright peaks clearly show the dominant wave system with the 180° ambiguity inherent in these observations.

The phase spectrum of Plate 2 is in units of (radians/wave number)^2. This is converted to a velocity spectrum by the relation between interferogram phase and scattering element line-of-sight velocity:

$$\Phi = 2\pi \frac{\beta}{\lambda} \frac{u}{v}$$

where Φ is the interferogram phase, β is the antenna spacing, λ is the radar wavelength, u is the line-of-sight velocity component of the scattering element, and v is the aircraft velocity.

A further conversion is needed to obtain the wave-driven orbital velocity from the observed line-of-sight velocity. This factor is purely geometric and depends on the direction that the wave is traveling relative to the aircraft, hence it is most easily derived from the spectra. This factor, G, is [*Alpers and Rufenach*, 1979]

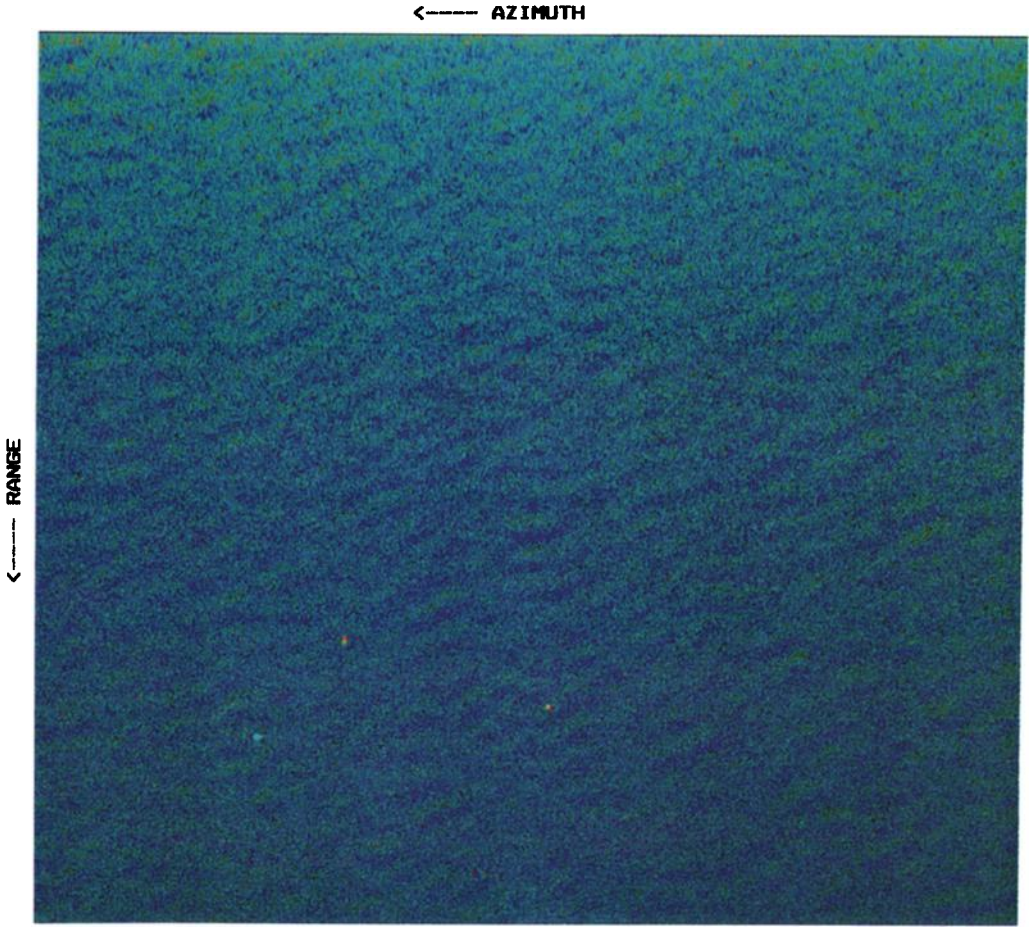

Plate 1. The dual antenna interferogram of the ocean surface. Aircraft motion was to the left along the top of the image, which is the along-track or azimuth direction. The aircraft heading was 202°. The bright spots in the lower corner are floating instrument platforms (FLIP) and three ships associated with the Surface Wave Process Program experiment.

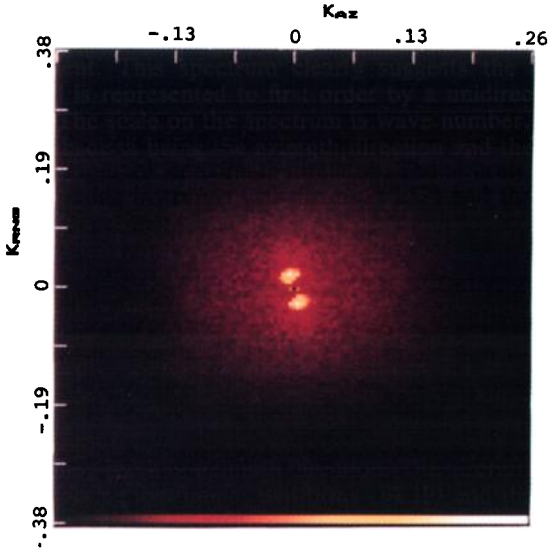

Plate 2. The two-dimensional wave spectrum obtained from the interferogram. The two sharp spectral peaks show the 180° directional ambiguity associated with this type of measurement. This spectrum clearly suggests the ocean wave field is represented to first order by a unidirectional sinusoid. The scale on the spectrum is wave number, m^{-1}, with the abscissa being the azimuth direction and the ordinate range.

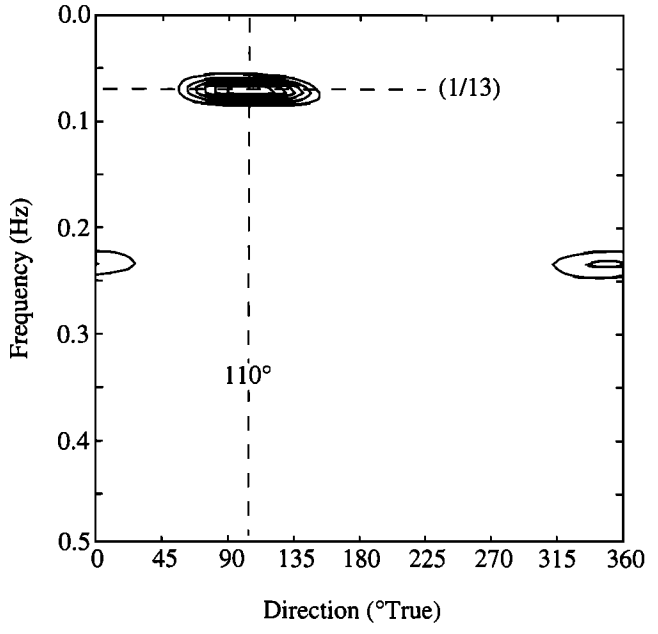

Figure 1. The directional spectrum obtained by the acoustic Doppler wave meter aboard FLIP. Mean direction is 110°, and wave period is estimated to be 13 s. The higher-frequency local wind-wave peak is associated with periods of approximately 4 s and with the true south direction. The broadness of both peaks in the directional domain is due to the course resolution analysis used in this example.

$$G = \sqrt{\sin^2 \alpha + \frac{z^2}{\rho^2} \cos^2 \alpha}$$

where z is the aircraft altitude, ρ is the slant range, and α is the angle between the aircraft velocity and the direction of the ocean wave.

The angular velocity of each orbiting scattering element, which is the same as the angular frequency of the wave, is related to the ocean wavelength, L, by the dispersion equation

$$\omega = \sqrt{\frac{2\pi g}{L}}$$

where g is the acceleration due to gravity. L is obtained, of course, from the spectrum, and the wave height is simply the ratio of the orbital velocity to the angular velocity.

We have integrated the area of the peaks of Plate 2 to obtain the total "energy" (i.e., phase squared) of the wave system but have not included the pedestal upon which the peaks sit. Although the ocean can be expected to have components of wide band noise, the radar measurements themselves must produce most of this observed noise. This results from the fact that the two interferometer measurements are separated by a small interval of time, 0.045 s, and during that time, the distribution of reflecting elements changes enough to cause decorrelation of the received phases. The result is an additional small, but not negligible, noise term.

Results of the three flight lines and the in situ wave staff observations on board FLIP are given in Table 1, along with the radar parameters.

The directional properties of the waves were obtained directly from the two-dimensional spectrum and knowledge of the plane heading. Prior to this, we had to correct for the distortion in the SAR spectra caused by scanning. That is, as the aircraft crosses the scene, the motion of the waves themselves causes a change in the observed along-track component of the wavelength. This change is of the order of the ratio of the wave phase velocity to the aircraft velocity. For our data, the worst case effect was a rotation of the spectrum by about 5°. The remaining directional ambiguity in possible wave direction was resolved by simply noting that the SWAPP experiment was just off the coast of California. Therefore the waves were traveling toward the east.

The three estimates of wave direction obtained from the radar are in excellent agreement with the directional estimates obtained by the sonar.

We note that the waves were traveling in essentially the range direction in the first column, in the azimuth direction in the third column, and halfway between in the second column. The measured wave heights agree reasonably well for the three cases. The azimuth falloff phenomenon did not affect the results for the long, shallow waves observed here.

5. Sonar Results

For the present comparison a "quick look" analysis of the sonar data is used [*Smith*, 1992, also manuscript in preparation, 1993]. Directional resolution is traded for speed and robustness: estimates can be formed from as little as 3 min of data. The directionally integrated results compare favorably with nondirectional frequency spectra formed from resistance wire data (Figures 1 and 2). A brief description of the technique follows; a detailed discussion is presented by J. A. Smith (manuscript in preparation, 1993).

To form these quick look results, 150 m of data from each of the four beams is used, spanning the range from 75 m to 225 m from FLIP (50 independent range bins). Velocity estimates from 1024 pings (768 s) are used, starting at 1317 PST, March 16, 1990. First, a two-dimensional fast Fourier transform is performed on the time-range matrix of data from each beam. A 256-point $\cos^2$ window is employed in time, offset by 128 points for successive estimates (which are averaged together). Then the 50 points in range are $\cos^2$ windowed and zero padded to 64 points. The estimate for each wavenumber is weighted by an amount equivalent to $\cos^2 \theta$, where θ corresponds to the angle between the beam and the surface wave, defined by the ratio of the range component of wavenumber to the wavenumber magnitude from frequency, using linear dispersion. The weighted power estimates are separated into $+k$ (outgoing) and $-k$ (incoming) parts, and each part is summed. Since the velocity estimates are already effectively weighted by $\cos^2 \theta$, the resulting sums are equivalent to $\cos^4 \theta$ weighted directional integrals. The net result is 8 $\cos^4$ weighted estimates for each frequency, distributed at 45° increments in direction. The effects of range-mean removal, especially at the lower frequencies, were compensated for through simulation. This results in a "calibration coefficient" for each frequency. This correction becomes too large for frequencies below about 1/(16 s), given the inherent noise level of the measurements; thus the estimates below this frequency should be disregarded. These results are relatively insensitive to the most important degrading effect present, the heading varia-

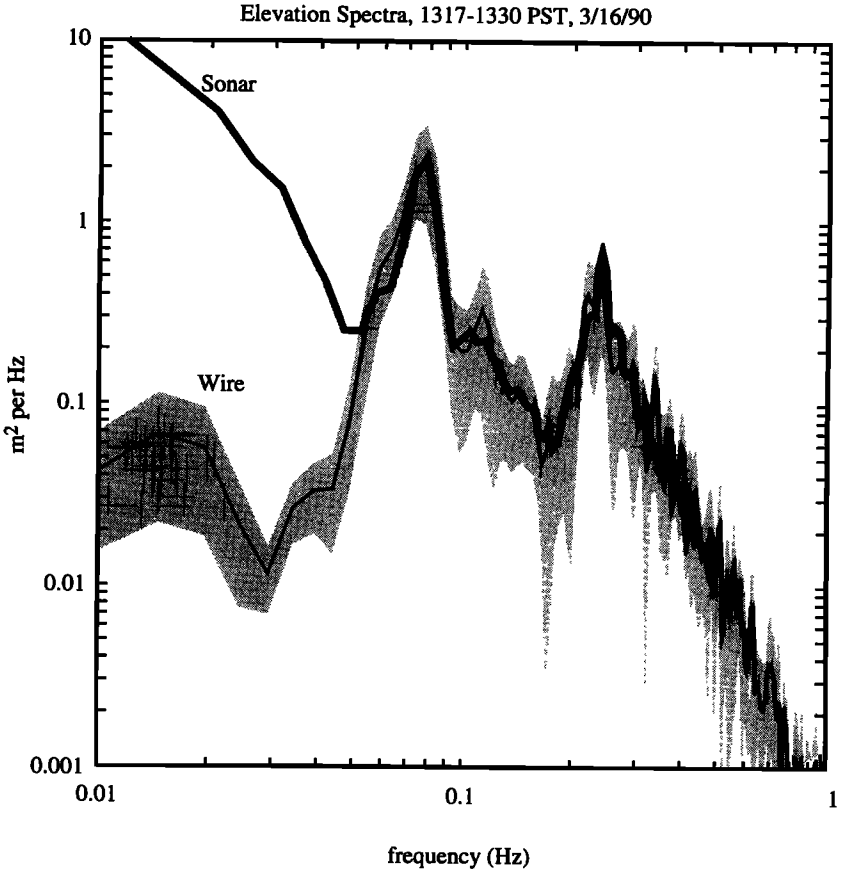

Figure 2. The power spectrum obtained by a conventional wave staff aboard FLIP. Note the sharp peak at the wave period of approximately 13 s. The local high-frequency wind wave peak is seen to occur for wave periods in the range of 4–5 s. Note that waves of that short a length are not visible to the radar and hence do not appear in Plate 2.

tions of FLIP (of the order of 5° rms). The resulting directional information is sufficient to estimate the 0th (power) through 3rd (skewness) moments of the directional distribution. (In comparison, tilt and roll buoys provide estimates of the 0th through 2nd moments).

The results are projected for display onto a grid with 5° spacing in direction, using the (generalized) inverse of the $\cos^4 \theta$ basis functions (Figure 1). This yields negative energy sidelobes, but these do not interfere with visual interpretation of the results. As seen in both Plate 2 and Figure 1, there were two "peaks" in the surface wave spectra at the time of the comparison (1317–1330 PST, March 16, 1990): a lower-frequency "swell peak" and a higher-frequency "local seas" peak. The largest directional estimate corresponds to a 12.8-s period (±0.4), propagating toward 110° true (±2.5°). The local wind wave peak occurs at a 4.2-s period (±0.05), propagating toward 350° true (±2.5°).

The acoustic Doppler system aboard FLIP, like the interferometer technique, shows a swell spectrum with a peak near a 13-s period and a direction of approximately 110°). The power spectrum from the wave staff on FLIP (Figure 2) shows the sharp peak characteristic of pure swell conditions, that also has a period of 13 s. It is clear that both novel wave measuring devices have obtained the same numerical description of the wave field, and that these estimates compare well with traditional measurements.

6. Conclusions

In summary, the results we have reported are reasonably consistent for aircraft measurements from different flight lines and for both the conventional in situ and sonar measurements. Furthermore, measurements of the waves traveling in the along-track direction were reasonably consistent with the measurements made when the same waves were traveling across track. The azimuth cutoff [*Lyzenga and Bennett*, 1991; *Rufenach et al.*, 1991] did not affect these data, since the ocean wavelength was long and the wave height was small.

It is interesting to note that the Doppler sonar and interferometric SAR measurements are based on much the same physical principals. Both techniques involve estimating velocities from Doppler-like shifts in the frequency of the backscattered wave (sound waves for the sonar and radio waves for the SAR). The scatterers are short surface waves for the SAR, so the phase velocity of the scattering waves is added to the estimates (as noted above). The sonar signal scatters from subsurface bubbles, giving an effective measurement depth of about 1 m, but with negligible additional velocity (the scattering bubbles are very small and rise very slowly).

Both share the same form of geometric correction for projecting the range component of velocity onto the plane of wave motion, and both are "blind" to wave motion that is exactly

perpendicular to the measurement beam. The sonar system makes use of measurements along 4 different directions, so the combined estimate of directional wave spectra has no blind spots. In the SAR case, because of the aircraft's altitude above the surface, the line-of-sight is never perpendicular to the plane of wave motion. Thus the blind spots do not occur.

Acknowledgments. The research described in this paper was carried out in part by the Jet Propulsion Laboratory, California Institute of Technology, under a contract with the National Aeronautics and Space Administration. The University of California, through the Scripps Institution of Oceanography and the Office of Naval Research through grant N00014-90-J-1285, also provided support for this work, as did NASA through grant NAGW-1952.

References

Alpers, W. R., and C. L. Rufenach, *IEEE Trans. Antennas Propag.*, *27*(5), 1979.

Alpers, W. R., D. B. Ross, and C. L. Rufenach, The detectability of ocean surface waves by real and synthetic aperture radars, *J. Geophys. Res.*, *86*, 6481–6498, 1981.

Crawford, C. B., and D. M. Farmer, On the spatial distribution of ocean bubbles, *J. Geophys. Res.*, *92*, 8231–8243, 1987.

Emmanuel, C. B., and P. A. Mandics, A feasibility study for the remote measurement of underwater currents using acoustic Doppler techniques, *NOAA Tech. Rep., ERL 278-WPL25*, 1–36, 1973.

Goldstein, R. M., and H. A. Zebker, Interferometric radar measurement of ocean surface currents, *Nature*, *328*, 707–709, 1987.

Goldstein, R. M., T. P. Barnett, and H. A. Zebker, Remote sensing of ocean currents, *Science*, *246*, 1282–1285, 1989.

Hasselmann, K., R. K. Raney, W. Plant, W. Alpers, R. Shuchman, D. Lyzenga, C. Rufenach, and M. Tucker, Area of synthetic aperture radar ocean imaging: A MARSEN view, *J. Geophys. Res.*, *90*, 4659–4686, 1985.

Jackson, F. C., An analysis of short pulse and dual frequency radar techniques for measuring ocean wave spectra from satellites, *Radio Sci.*, *16*, 1385–1400, 1989.

Lyzenga, D. R., and J. R. Bennett, Estimation of ocean wave spectra using 2-antenna SAR systems, *IEEE Trans. Geosci. Remote Sens.*, *29*(3), 463–465, 1991.

Miller, K. S., and M. M. Rochwarger, A covariance approach to spectral moment estimation, *IEEE Trans. Inf. Theory*, *IT-18*, 588–596, 1972.

Pinkel, R., The use of Doppler sonar for internal wave measurement, *Deep Sea Res.*, *28A*, 269–289, 1981.

Pinkel, R., and J. A. Smith, Repeat sequence codes for improved performance of Doppler sounders, *J. Atmos. Oceanic Technol.*, *9*, 149–163, 1992.

Pinkel, R., and F. N. Spiess, Space-time measurement of oceanic motions from a range-gated Doppler sonar, *J. Acoust. Soc. Am.*, *59*, suppl. 1, 58, 1976.

Raney, R. K., Wave orbital velocity, fade and SAR response to azimuth waves, *IEEE J. Oceanic Eng.*, *OE-6*(4), 140–146, 1981.

Rufenach, C. L., R. Shuchman, N. P. Malinas, and J. A. Johannessen, Ocean wave spectral distortion in airborne synthetic aperture radar imagery during the Norwegian continental shelf experiment of 1988, *J. Geophys. Res.*, *96*, 10,453–10,466, 1991.

Smith, J. A., Doppler sonar and surface waves: Range and resolution, *J. Atmos. Oceanic Technol.*, *6*, 680–696, 1989.

Smith, J. A., Observed growth of Langmuir circulation, *J. Geophys. Res.*, *97*, 5651–5664, 1992.

Stewart, R., *Methods of Satellite Oceanography*, 352 pp., University of California Press, Berkeley, 1985.

Thorpe, S., Bubble clouds: A review of their detection by sonar, of related models, and of how Kv may be determined, in *Oceanic Whitecaps*, pp. 57–68, D. Reidel, Norwell, Mass., 1986.

Walsh, E. J., D. Hancock, and D. Hines, Directional wave spectra measured with a surface contour radar, *J. Phys. Oceanogr.*, *14*, 566–592, 1985.

Weller, R. A., M. A. Donelan, M. G. Briscoe, and N. E. Huang, Riding the crest: A tale of two wave experiments, *Bull. Am. Meteorol. Soc.*, *72*, 163–183, 1991.

T. P. Barnett, R. Pinkel, and J. Smith, Scripps Institution of Oceanography, University of California, La Jolla, CA 92093.

R. M. Goldstein and F. Li, Jet Propulsion Laboratory, MS 300-227, 4800 Oak Grove Dr., Pasadena, CA 91109.

(Received February 18, 1992; revised October 13, 1993; accepted October 26, 1993.)